Comparative Study of Various Mechanisms for Metallocene-Catalyzed α-Olefin Polymerization

Iñaki Silanes and Jesus M. Ugalde

Kimika Fakultatea, Euskal Herriko Unibertsitatea and Donostia International Physics Center (DIPC), P.K. 1072, 20080 Donostia, Euskadi, Spain

Received April 20, 2005

In this paper we try to give answers to some unexplained flaws in the widely accepted Cossée−Arlman mechanism (CAM) for the propagation step of the polymerization of α-olefins. We first take the bare cationic catalyst and make a comparison of the CAM with the so-called *Trigger* mechanism (TM) proposed by Ystenes, and not only see whether the latter model can predict, qualitatively, some reaction behaviors not explained by the former one but also theoretically calculate both reaction paths and make a quantitative comparison, in terms of reaction free energy. It turns out that, while in terms of electronic energy the TM is favored, inclusion of free energy corrections gives a lower energy profile for the CAM reaction path. We then make use of a model for an experimentally used catalyst counterion and study how it affects the reactivity of the metallocenic cation fragment toward the monomer.

1. Introduction

More than 45 years after the first olefin polymerizations by Ziegler−Natta type catalysts,[1,2] and 40 after Cossée and Arlman formulated their widely accepted two-step mechanism (see Figure 1) for the propagation step of this kind of reaction,[3−7] there still remain some unanswered questions.

A very important one is whether the π-complex exists, i.e., whether the complexation of the vinyl monomer to the catalyst fragment is a true minimum on the reaction potential energy surface (PES). Related to this, the presence of an insertion barrier is also under debate.

Early work by Morokuma (who has been very active in the field[8−13]) et al. on the ethylene + $[Cl_2TiCH_3]^+$ system[8] predicted a π-complex optimized at the Hartree−Fock (HF) level of theory. *Single-point* energy calculations at the second-order Moller−Plesset (MP2) theory level on the HF geometry gave a binding energy of 56.6 kcal/mol.

They also studied the silylene-bridged $[H_2SiCp_2ZrCH_3]^+$ + ethylene system[9] and predicted a π-complex with a restricted Hartree−Fock (RHF) binding energy of 19.1 and 33.5 kcal/mol at the restricted MP2 (RMP2) level of theory. An insertion transition state (TS) was also found, giving rise to an insertion barrier of 16.7 kcal/mol at the RHF level and 6.0 kcal/mol at the RMP2 level.

Similar results were obtained by Ziegler et al.,[14] using DFT methods. They came up with a π-complex with a 23 kcal/mol binding energy for ethylene + $[Cp_2TiCH_3]^+$ and around 26 kcal/mol for ethylene + $[H_2SiCp_2ZrCH_3]^+$. However their insertion barriers were small, namely, less than 1 kcal/mol for both of them.

Later work by Ahlrichs et al.[15] on both ethylene + $[Cp_2TiCH_3]^+$ and ethylene + $[Cl_2TiCH_3]^+$ stressed the importance of including electron correlation even in the geometry optimization step, lest *qualitatively* incorrect results be obtained. They claimed having avoided this problem by optimizing the geometries with the MP2 method, at which level they predicted a strictly downhill insertion of ethylene in the Ti−C bond (i.e., no π-complex nor insertion TS) for the ethylene + $[Cp_2TiCH_3]^+$ system. This result was rationalized by stressing how efficiently α-H agostic interactions reduce the steric hindrance to ethylene approach. For $[Cl_2TiCH_3]^+$ agostic interactions seemed to be weaker (or absent), and thus a π-complex and an insertion TS were indeed found.

In a pioneering paper, Buda et al.[16] treated the insertion of ethylene into $[H_2SiCp_2ZrCH_3]^+$ (same system as in one of the articles by Morokuma et al.[8]) by Car−Parrinello ab initio molecular dynamics (AIMD). This approach has the interesting advantage that it is not the electronic energy space that is analyzed, but the free energy one, that is, the actual hypersurface in

(1) Ziegler, K.; Hozkampf, E.; Breil, H.; Martin, H. *Angew. Chem.* **1955**, *67*, 541.
(2) Natta, G. *J. Polym. Sci.* **1955**, *16*, 143.
(3) Cossée, P. *Tetrahedron Lett.* **1960**, *17*, 12.
(4) Cossée, P. *J. Catal.* **1964**, *3*, 80.
(5) Arlman, E. J. *J. Catal*, **1964**, *3*, 89.
(6) Arlman, E. J.; Cossée, P. *J. Catal*. **1964**, *3*, 99.
(7) Arlman, E. J. *J. Catal.* **1966**, *5*, 178.
(8) Kawamura-Kuribayashi, H.; Koga, N.; Morokuma, K. *J. Am. Chem. Soc.* **1992**, *114*, 2359.
(9) Kawamura-Kuribayashi, H.; Koga, N.; Morokuma, K. *J. Am. Chem. Soc.* **1992**, *114*, 8687.
(10) Yoshida, T.; Koga, N.; Morokuma, K. *Organometallics* **1995**, *14*, 746.
(11) Musaev, D. G.; Froese, R. D. J.; Svensson, M.; Morokuma, K. *J. Am. Chem. Soc.* **1997**, *119*, 367.
(12) Froese, R. D. J.; Musaev, D. G.; Morokuma, K. *J. Mol. Struct. (THEOCHEM)* **1999**, *121*, 461.
(13) Das, P.; et al. In *Transition State Modeling for Catalysis*; Truhlar, D. G., Morokuma, K., Eds.; ACS Symp. Ser. 721; American Chemical Society, 1998.
(14) Woo, T. K.; Fan, L.; Ziegler, T. *Organometallics* **1994**, *13*, 2252.
(15) Weiss, H.; Ehrig, M.; Ahlrichs, R. *J. Am. Chem. Soc.* **1994**, *116*, 4919.
(16) Meier, R. J.; van Doremaele, G. H. J.; Iarlori, S.; Buda, F. *J. Am. Chem. Soc.* **1994**, *116*, 7274.

10.1021/om0503139 CCC: $30.25
Publication on Web 05/19/2005

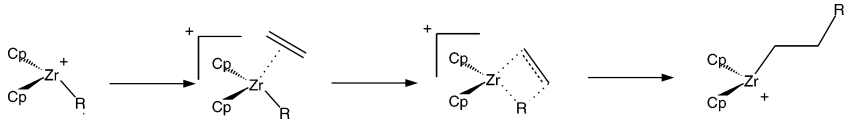

Figure 1. Cossée−Arlman mechanism.

which chemical reactions take place. The remarkably short reaction time span they obtained (∼150 fs) led them to conclude that a very low or no energy barrier at all was present in the monomer insertion. A second study on the same system,[17] but at different temperatures, further supported this idea, since the reaction time span turned out to be quite independent of the temperature.

Nevertheless, another paper by Morokuma et al.[10] questioned the aforementioned ones. Although RMP2//RHF (RMP2 single-point energy at RHF-optimized geometries) made Ahlrichs et al.[15] consider a downhill PES, similar calculations with the much more sophisticated restricted singlets and doublets configuration interaction with correction for quartets (RQCISD) level of theory (that is, RQCISD//RHF energies) applied to $[H_2SiCp_2MCH_3]^+$ (M = Ti, Zr, Hf) led Morokuma et al. to conclude that there actually exists a π-complex (with a RQCISD//RHF binding energy of 29.1 kcal/mol for M = Zr) and also a subsequent insertion TS, although with a low activation energy (9.4 kcal/mol in the case of M = Zr, at the RCISD//RHF level). They regarded the MP2 results by Ahlrichs et al. as "an artifact" and blamed the absence of barrier in the AIMD simulations by Buda et al. on an overstimation of the correlation energy by the LDA method; thus (they hypothesized) the TS disappeared because it was unrealistically stabilized at that theory level. While this artificial stabilization effect may well be present, we would like to emphasize that the AIMD calculations explore the reaction free energy, not the electronic energy. Thus there would be no contradiction in the prediction of the existence of an electronic energy insertion barrier and none in the free energy surface.

Some questions related to the Cossée−Arlman mechanism have been addressed by Ystenes. He proposed an alternative mechanism referred to as the *Trigger* mechanism (TM),[18,19] although in more recent papers Ystenes seems to get back to giving credit to the model by Cossée and Arlman.[20]

The main change the Trigger model introduces in the CAM is to propose the catalytic action of a second monomer unit for the insertion of a given monomer in the growing chain attached to the metallic center (see Figure 2). The idea is not new, as Ystenes himself makes clear (see refs 21−24 in ref 18), but it is in his papers where the idea has been properly placed into perspective for the first time.

We would like to emphasize that both the model by Cossée and Arlman and that by Ystenes were developed for Ziegler−Natta catalysts. Both Kaminsky[21,22] and

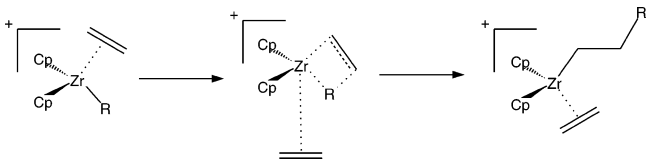

Figure 2. Trigger mechanism.

Corradini[23,22] have translated the CAM to metallocenic catalysts, with little, if any, fundamental change. While some details may vary, the problems we will discuss here are essentially equivalent for both the heterogeneous and the homogeneous branch of these metallic catalyst families. Moreover, many recently discovered post-metallocenic catalysts[11,24,25] possibly follow similar reaction steps.

The calculations presented in the first section have been carried out for the "bare" metallocene cation, without any explicit effect of the counterion (e.g., methylaluminoxane anion, MAO^-), beyond the implicit activation of the metallocene itself. The hypothesis that the primary effect of the MAO is to activate a metallocene precursor (usually a dichloride), giving rise to a cationic molecule, which is the active species, is assumed in many papers and was experimentally confirmed by Yang et al.[26] for zirconocenes and Eish et al.[27] for titanocenes.

Nevertheless the effect of the counterion is still under debate. Thus while some authors[28,29] suggest that the effect of the cocatalyst anion is not negligible and should be included explicitly in the calculations (for example in the form of boron compounds), others[30] justify the neglect of counterions in simulations. Consequently, we have devoted a second part of our work to include a model for $[CH_3B(C_6F_5)_3]^-$, a moiety that has been widely used as a molecularly well-defined counterion (as opposed to the structurally unknown MAO) in olefin polymerization, both experimentally[26,31−33] and theoretically.[28,34,35]

(17) van Doremaele, G. H. J.; Meier, R. J.; Iarlori, S.; Buda, F. *J. Mol. Struct. (THEOCHEM)* **1996**, *363*, 269.
(18) Ystenes, M. *J. Catal.* **1991**, *129*, 383.
(19) Ystenes, M. *Makromol. Chem. Macromol. Symp.* **1993**, *66*, 71.
(20) Thorshaug, K.; Stovneng, J. A.; Rytter, E.; Ystenes, M. *Macromol.* **1998**, *31*, 7149.
(21) Kaminsky, W.; Steiger, R. *Polyhedron* **1988**, *7* (22/23), 2375.
(22) Ochoteco, E. Polimerización de propileno con catalizadores de metaloceno. Ph.D. Diss., University of the Basque Country, 2001.
(23) Corradini, P.; Guerra, G. *Prog. Polym. Sci.* **1991**, *16*, 239.
(24) Deng, L.; Margl, P.; Ziegler, T. *J. Am. Chem. Soc.* **1997**, *119*, 1094.
(25) Lanza, G.; Fragala, I. L.; Marks, T. J. *Organometallics* **2002**, *21*, 5594.
(26) Yang, X.; Stern, C. L.; Marks, T. J. *J. Am. Chem. Soc.* **1991**, *113* (9), 3623.
(27) Eisch, J. J.; Caldwell, K. R.; Werner, S.; Krueger, C. *Organometallics* **1991**, *10*, 3417.
(28) Chan, M. S. W.; Ziegler, T. *Organometallics* **2000**, *19*, 5182.
(29) Nifant'ev, I. E.; Ustynyuk, L. Y.; Laikov, D. N. *Organometallics* **2001**, *20*, 5375.
(30) Philipp, D. M.; Muller, R. P.; III, W. A. G.; Storer, J.; McAdon, M.; Mullins, M. *J. Am. Chem. Soc.* **2002**, *124*, 10198.
(31) Chen, M.-C.; Roberts, J. A. S.; Marks, T. J. *J. Am. Chem. Soc.* **2004**, *126* (14), 4605.
(32) Landis, C. R.; Sillars, D. R.; Batterton, J. M. *J. Am. Chem. Soc.* **2004**, *126*, 8890.
(33) Strauch, J. W.; Faure, J.-L.; Bredeau, S.; Wang, C.; Kehr, G.; Frohlich, R.; Luftmann, H.; Erker, G. *J. Am. Chem. Soc.* **2004**, *126* (7), 2089.
(34) Vanka, K.; Ziegler, T. *Organometallics* **2001**, *20*, 905.
(35) Song, F.; Lancaster, S. J.; Cannon, R. D.; Schormann, M.; Humphrey, S. M.; Zuccaccia, C.; Macchioni, A.; Bochmann, M. *Organometallics* **2005**. ASAP Article, DOI 10.1021/om049248d.

It is also worth noting that there are many side reactions relevant for the propagation reaction (e.g., production of "dormant" bimolecular species[36]) and that the whole polymerization process is much more complex than what we outline here. Our concern, though, is to model the propagation reaction of active catalytic centers.

2. Selected Characteristics of Metallocene-Catalyzed α-Olefins

We will refer here only to the three issues we consider most important about the reactions under consideration. These issues have already been put forward by Ystenes in his papers,[18,19] among a couple of others, being regarded as conflicting points for the CAM for Ziegler–Natta catalysts, and we extend them to metallocenic catalysts.

2.1. The Reaction Rate Order of the Monomer Predicted by Theory Does Not Match Experiment. It is widely accepted that most metallocene-catalyzed polymerizations have reaction rates proportional to the monomer and catalyst concentrations, i.e., are of first order with respect to both the monomer and the catalyst. The problem here is that the CAM suggests that the propagation reaction takes place in two steps (complexation and insertion of the monomer), and chemical intuition indicates that the second one is most likely the slowest one, since the first one has no barrier and so it is expected to be very fast. If it were the case, then a comparison with a typical *Michaelis–Menten* reaction mechanism (eq 1) would show that the reaction rate would be of first order with respect to the catalysts, but of zeroth order (i.e., independent) with respect to monomer. This is ilustrated in the Michaelis–Menten kinetic equation (eq 2), where $v = k_2$[Catalyst] if $k_1 > > > k_2$. Linear proportionality for monomer seems to be reasonable only if the first step (complexation) is much slower than the second one (insertion). Following eq 2, $v = k_1$[Catalyst][Substrate] if $k_1 < < < k_2$. The latter is highly counterintuitive.

$$\text{Catalyst} + \text{Substrate} \underset{k_{-1}}{\overset{k_1}{\rightleftharpoons}} \text{Complex} \underset{k_{-2}}{\overset{k_2}{\rightleftharpoons}} \text{Product} \quad (1)$$

$$v = \frac{k_2[\text{Catalyst}]}{1 + \dfrac{k_{-1} + k_2}{k_1[\text{Substrate}]}} \quad (2)$$

2.2. The Effect of Lewis Bases (including MAO^- counterion) Is Controversial. It is quite straightforward that Lewis bases that may be present in the medium (one of them being the MAO^- counterion for the catalyst cation) should compete for the empty site in the coordination sphere of the metal formed in various steps of the CAM. Vanka and Ziegler[34] studied this scenario by computational means (DFT calculations). They calculated the formation enthalpies of the complexes formed by the bare catalyst cation and some other Lewis bases, namely, zirconocenic precatalyst itself ($Cp_2Zr(CH_3)_2$), solvent (toluene), cocatalyst ($B(C_6F_5)_3$), and $Al(CH_3)_3$. Although all of them produced stable complexes, none would bind stronger than the counterion $[B(C_6F_5)_3CH_3]^-$, so they also studied the possibility of forming "sandwich" species, that is, the Lewis base inserted between the aforementioned cation and counterion.

Comparing the results with those obtained with the monomer (ethylene) for Lewis base, they concluded that dormant species formed by complexation of these Lewis bases with the catalyst could compete successfully with ethylene complexes, but for longer growing polymer chains (modeled by a propyl instead of a methyl attached to the zirconium atom), the complexation of the monomer was deemed closer in energy (probably due to steric effects) to that of Lewis bases. It should be noted that this would match the experimental results, where usually the propagation rate is smaller at the beginning of the polymerization (presumably due to greater abundance of dormant species; increasing the growing polymer chain length would make the monomer more and more favored over other Lewis bases). In the case of sandwiched species, ethylene seemed to bind more strongly in its corresponding sandwich than the solvent, but not more than the $Al(CH_3)_3$; therefore the latter could well inhibit the catalysis process (anyway its concentration, when used as scavenging agent, should be significantly lower than that of the monomer).

2.3. The Growing Chain Flipping Behavior Is Still Unexplained. It is widely accepted that in metallocenic catalytic systems each metallic center has two coordination positions active for the polymerization reaction. In every insertion step, the growing polymer chain is attached to one of them, and the incoming monomer binds to the other one. The possibility of obtaining isotactic or syndiotactic polymer is explained by how the monomers tend to bind to these coordination sites. Given that these two coordination sites will favor the complexation (and subsequent insertion) of the monomer with either equivalent or opposite side group (e.g., methyl group in propylene) arrangement, one can assume that the first case will produce an isotactic polymer (Figure 3), and the second one a syndiotactic one (Figure 4), provided that the monomer complexations happen in a coordination-site alternating fashion.[37] Of course, if neither of them favors a given orientation of the monomer, the product will be atactic.

It is important to note that the growing chain has to flip once (or an odd number of times) per monomer insertion. A successful theoretical mechanism has to be able to account for this fact and explain not only how the flip happens when the monomer inserts itself, but also why the chain stays in place between two succesive insertions (or flips exactly an even number of times). If the growing chain stays in the same coordination site all the time, then both isotactic and atactic products can be rationalized, but no easy explanation can be given to the formation of syndiotactic polymers with a static growing chain, nor with an uncontrolled flipping of the chain. Anyway, some authors[38] have taken into account the possibility of chain flipping between succesive insertions and have come up with the conclusion that for some catalytic systems the inversion (flip) rate can even be much higher than the monomer insertion rate.

(36) Song, F.; Cannon, R. D.; Bochmann, M. *J. Am. Chem. Soc.* **2003**, *125* (25), 7641.

(37) Bierwagen, E. P.; Bercaw, J. E.; III, W. A. G. *J. Am. Chem. Soc.* **1994**, *116* (4), 1481.

(38) Mohammed, M.; Nele, M.; Al-Humydi, A.; Xin, S.; Stapleton, R. A.; Collins, S. *J. Am. Chem. Soc.* **2003**, *125* (26), 7930.

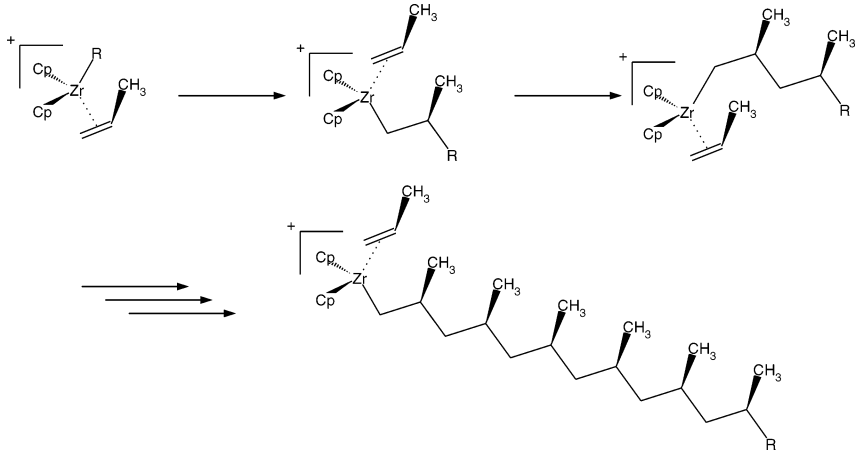

Figure 3. Isotactic growth.

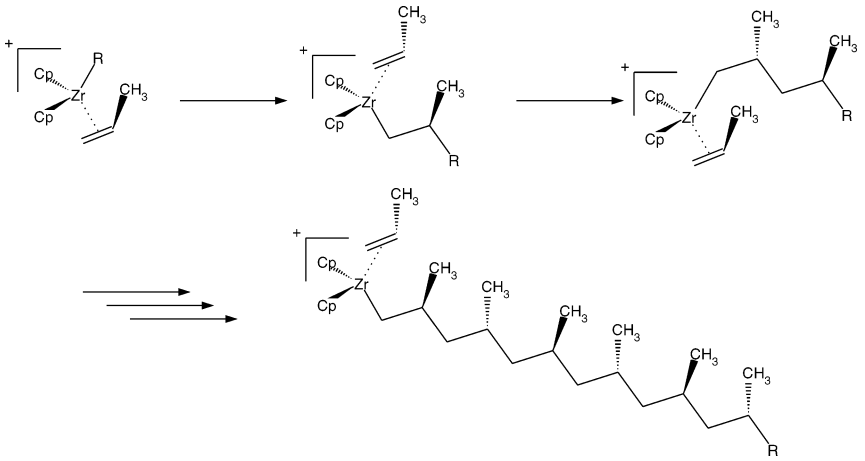

Figure 4. Syndiotactic growth.

3. Methods

Our first step is to use quantum calculations to sketch a potential energy surface (PES) for the approach of the monomer to the metal. Then more accurate calculations will be done on the stationary points, so that we can compare the heights of the energetic barriers for the propagation reaction.

For our calculations we have chosen $[Cp_2ZrCH_3]^+$ as the active catalyst and ethylene as the monomer, provided that they are the simplest species that can model the reaction and thus the less computationally demanding. The counterion $[CH_3B(C_6F_5)_3]^-$, when used, has been modeled by a $[CH_3B(CF_2Cl)_3]^-$ unit. The suitability of such a model will be discussed later.

All the calculations have been carried out using the GAUSSIAN 98 package[39] and the B3LYP density functional (DFT) method therein.

We have used four basis sets throughout this work. First, for the relaxed PES scans we chose the SKBJ effective core potential (ECP) basis set,[40−42] as defined in the Extensible Computational Chemistry Environment Basis Set Database.[43] We chose this basis set for performance considerations, since it has all of the core electrons described by pseudopotential functions, and only the valence shell of each element is described with Gaussian basis functions, thus reducing the computational expense considerably.

Second, for the geometry optimizations and subsequent frequency calculations we have made use of the LanL2DZdp basis set, which is an extension of the LanL2DZ basis set,[44−46] supplemented with diffuse and polarization functions.[47] Unfortunately there is no such extension for berillyum or zirconium, so we have used the bare LanL2DZ basis set for these elements. The LanL2DZ basis set is a pseudopotential one, as it is SKBJ, but with a smaller core described with ECPs, so that an expected increase in accuracy is achieved at the expense of an actual increase in computational cost.

Third, for the single-point energy calculations we used the widely known 6-311++G(3df,3pd) basis set, as implemented in Gaussian, for all the elements except for the zirconium, for which the SDD basis set was used, as implemented in Gaussian. We have called this basis set the TZ basis set throughout this paper.

Last, when testing for the relevance of diffuse functions for the description of a potential β-agostic interaction on the

(39) Frisch, M. J.; et al. *Gaussian 98*, a.11.3; Gaussian, Inc.: Pittsburgh, PA, 2002.

(40) Stevens, W. J.; Basch, H.; Krauss, M. *J. Chem. Phys.* **1984**, *81*, 6026.

(41) Stevens, W. J.; Krauss, M.; Bausch, H.; Jasien, P. G. *Can. J. Chem.* **1992**, *70*, 612.

(42) Cundari, T. R.; Stevens, W. J. *J. Chem. Phys.* **1993**, *98*, 5555.

(43) Basis sets were obtained from the Extensible Computational Chemistry Environment Basis Set Database, Version 02/25/04, as developed and distributed by the Molecular Science Computing Facility, Environmental and Molecular Sciences Laboratory, which is part of the Pacific Northwest Laboratory, P.O. Box 999, Richland, WA 99352, and funded by the U.S. Department of Energy. The Pacific Northwest Laboratory is a multi-program laboratory operated by Battelle Memorial Institute for the U.S. Department of Energy under contract DE-AC06-76RLO 1830. Contact David Feller or Karen Schuchardt for further information.

(44) Dunning, T. J., Jr.; Hay, P. J. *Methods of Electronic Structure Theory*; Plenum Press: New York, 1977; Vol. 2.

(45) Hay, P. J.; Wadt, W. R. *J. Chem. Phys.* **1985**, *82*, 270.

(46) Ortiz, J. V.; Hay, P. J.; Martin, R. L. *J. Am. Chem. Soc.* **1992**, *114*, 2736.

(47) Check, C. E.; Faust, T. O.; Bailey, J. M.; Wright, B. J.; Gilbert, T. M.; Sunderlin, L. S. *J. Phys. Chem. A* **2001**, *105*, 8111.

zirconium atom, we used both the LanL2DZ basis set and an extension of it consisting in the inclusion of a diffuse function in the β-carbon and its three hydrogens (a total of four extra s functions). We refer to the latter as LanL2DZβ. Additionally, SKBJ and LanL2DZdp basis sets have also been used, the latter only in the simplest of the two cases studied in this test.

These computational details and the species taken into account are not so different from those studied by Thorsaug et al.,[20] but additionally we have performed frequency calculations in order to obtain reaction Gibbs free energies, something they did not do due to computational limitations. Of course, temperature is a factor in the entropic part of ΔG. The numbers we give here are calculated at 298 K, which is a reasonable temperature for this kind of polymerization.

It is also noteworthy that we have performed such frequency calculations on all the stationary points, coming up successfully with real frequencies for all the normal modes in the case of local minima and only one imaginary frequency for the transition states. We have also confirmed that in every case the imaginary frequency corresponded to the desired normal mode.

With regard to the flipping of the growing chain, we have modeled it with a typical bridged zirconocene, namely, the *ansa*-ethylene-bis(indenil) methyl zirconium cation, while the oscillating chain has been reduced to a simple methyl group.

For the ball-and-stick graphical representation of molecules, the Raster3D software[48] has been extensively used throughout this article. The schematic molecular representations have been produced with ChemTool.[49] Various graphs and schematic figures have been produced with Grace[50] and Xfig.[51]

4. Results and Discussion

4.1. Description of the β-Agostic Interaction. It has been argued that an agostic interaction between the β-hydrogen and the zirconium is formed and that its description is crucial. Although our calculations with ethyl chains in bare cations suggest that this agostic interaction does exist, when introducing the counterion in the system its importance seems to decrease drastically (see Figure 6).

The underlying question is not only whether the length of the growing polymer chain affects the insertion of subsequent monomers (which sounds reasonable for very short chains and is probably irrelevant for longer chains), but also whether one should add diffuse functions in order to properly describe the possible agostic interactions by means of theoretical calculations, even in a *qualitative* way.

We have tested for the stability of these β-agostic interactions by performing a relaxed potential energy scan along the H−C−C−Zr dihedral angle, D, giving it values from 0° to 60°. The two limiting structures are depicted in Figure 5.

This PES scan was carried out on the bare catalyst cation and on the catalyst/counterion system, using three basis sets, namely, SKBJ, LanL2DZ, and LanL2DZβ, plus also the larger LanL2DZdp basis set for the bare catalyst. Figure 6 shows the result of the seven scans.

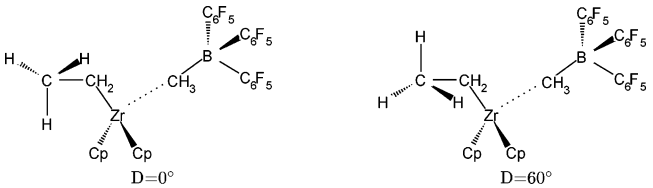

Figure 5. Two limit structures in the β-agostic interaction test scan.

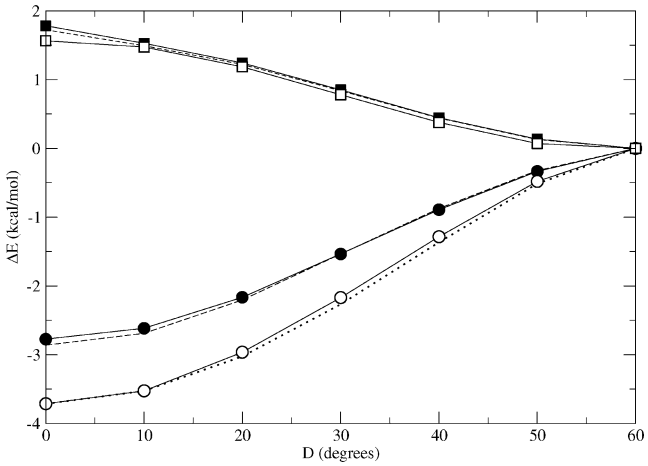

Figure 6. PES along the H−C−C−Zr dihedral angle for the bare catalyst cation (circles) and catalyst/counterion (squares) systems. LanL2DZ basis set results are represented by solid symbols, and SKBJ results by open ones. The dashed lines below each continuous line draw the corresponding LanL2DZβ results. The dotted line corresponds to LanL2DZdp values for bare catalyst. ΔEs are given with respect to the $D = 60°$ moiety.

Although the inclusion of diffuse functions on the subject atoms (LanL2DZβ basis set) increase very slightly the relative stability of the geometry with a planar H−C−C−Zr dihedral angle (either for the cation or the neutral system), it is clear that all basis sets regard the $D = 60°$ moiety as the most stable one for the neutral system and the $D = 0°$ geometry for the cation. When the larger LanL2DZdp basis set is used, the β-agostic geometry seems to be even more favored, and it seems reasonable to think that when including the counterion, the $D = 0°$ and $D = 60°$ geometries will be closer in energy. The basis set we use in the bulk of the article to calculate the different relaxed scans, that is, the small SKBJ, gives figures very close to the larger LanL2DZdp.

We can therefore conclude that the PES is quite flat for the rotation of the methyl end of the ethyl group, so that the possible β-agostic interaction cannot be considered too tightly binding for the cation and much less so for the neutral system. It is also apparent that the SKBJ basis set is suitable for a qualitative sketch of the PES along the monomer approach.

4.2. Bare Cation. 4.2.1. Monomer Approach PES Scan. We have performed some fully relaxed PES scans in the ethylene + $[ZrCp_2CH_3]^+$ system; that is, some internal variables (interatomic distances) were fixed at selected values, while all the remaining variables were freely optimized. The distances that were fixed in each scan are henceforth labeled as pseudo-reaction coordinates.

(48) Merrit, E. A.; Bacon, D. J. *Methods Enzymol.* **1997**, *277*, 505. *Raster3D* can be freely downloaded at: http://www.bmsc.washington.edu/raster3d/.

(49) Kroeker, M.; Banck, M.; Liboska, R.; Volk, T. *Chemtool 1.4.1*. Downloadable under the GPL license at: http://ruby.chemie.uni-freiburg.de/ martin/chemtool/chemtool.html.

(50) *Grace 5.1.18*. Downloadable under the GPL license at: http://plasma-gate.weizmann.ac.il/Grace/.

(51) Sutanthavibul, S.; Yap, K.; Smith, B.; King, P.; Boyter, B.; Sato, T. *Xfig 3.2.5*. Freely downloadable at: http://www.xfig.org/, 1985−2005.

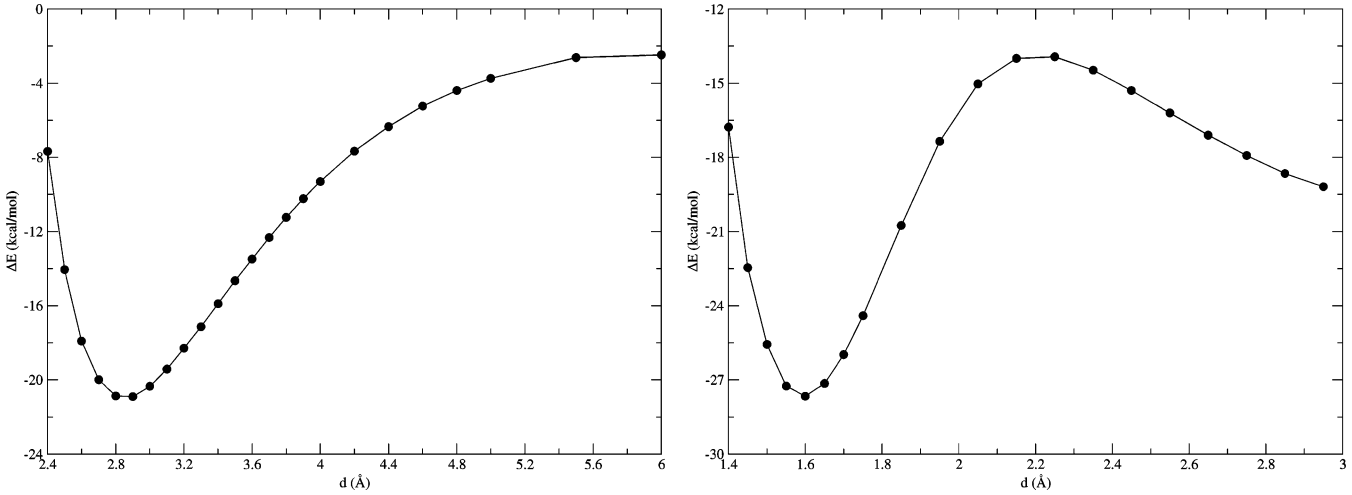

Figure 7. PES corresponding to varying the C_1-C_α (left) and $Zr-C_1C_2$ (right) distances for the bare zirconocene cation + ethylene system. Distances in Å and energies in kcal/mol.

First, we wanted to check whether a π-complex exists, that is, if there is a minimum in the PES corresponding to the approach of the monomer to the cation, *before* it inserts into the $Zr-C_\alpha$ bond. We chose the $Zr-C_1C_2$ distance as the pseudo-reaction coordinate to scan, where C_1 and C_2 are the carbon atoms of the ethylene. The X−YZ notation is used to indicate that both X−Y and X−Z are fixed and equal. We made this variable evolve from a far away distance (6 Å), where the binding energy (defined as the electronic energy of the complex minus the sum of those of the monomer and cation evaluated separately) is small (around 2.0 kcal/mol) and up to a little closer than the minimum energy point ($d(Zr-C_1C_2) = 2.4$ Å).

Second, once the monomer is close to the metallic center, we expect to observe a maximum in the PES corresponding to the approach of one of the carbon atoms of the monomer to the carbon of the methyl group of the cation (α-carbon of the growing polymer chain). In this case we have selected the C_1-C_α distance as the pseudo-reaction coordinate and calculated the resulting PES ranging from carbon−carbon distances closer than the equilibrium C−C single bond (around 1.54 Å) up to where the energy started decreasing after a maximum, namely, the insertion TS.

Inspection of Figure 7 confirms that there exists a π-complex when the olefin is at around 2.9 Å from the zirconium atom. It is also evident that an insertion TS must exist somewhere near $d(C_1-C_\alpha) = 2.2$ Å, and of course the product appears close to $d(C_1-C_\alpha) = 1.55$ Å.

In the case of the TM, we did not perform such a PES scan, but rather directly optimize the corresponding stationary points.

4.2.2. Relevant Stationary Structrures along the PES. We picked the relevant points of the PES scans in Section 4.2.1 and optimized their geometries with the LanL2DZdp basis set. We regarded as "relevant" the minimum of the $d(Zr-C_1C_2)$ scan (π-complex, CAM_{comp}) and the maximum (insertion TS, CAM_{TS}) and minimum (product, CAM_{prod}) of the $d(C_1-C_\alpha)$ scan, as well as the ethylene and zirconocene moieties infinitely separated (reactants, Et, and CAM_{reac}), and their energies were refined by means of single-point energy calculations with the TZ basis set. These geometries and the Cossée−Arlman mechanism energy profile are depicted in Figure 8. The energies are summarized in Table 1.

Table 1. Energy Differences and Gibbs Free Energy Differences (in kcal/mol) at Selected Stationary Points along the Cossée−Arlman Reaction Path[a]

	LanL2DZdp		TZ	
species	ΔE	ΔG	ΔE	ΔG
CAM_{reac} + Et	17.59	5.32	16.73	4.46
CAM_{comp}	0.00	0.00	0.00	0.00
CAM_{TS}	7.12	10.55	8.01	11.44
CAM_{prod}	−8.44	−4.03	−5.77	−1.36

[a] Values obtained by single-point calculations with the basis sets shown, on geometries optimized at the B3LYP/LanL2DZdp theory level.

A summary of the geometrical features of the CAM reaction path follows. An ethylene monomer unit approaches the CAM_{reac} catalyst cation, forming the CAM_{comp} π-complex without any intermediate TS to be found. In the π-complex the Zr−C distances for the monomer carbons are 2.862 and 2.855 Å. At this stage the C_1-C_2 double bond is barely affected, with a C_1-C_2 distance of 1.353 Å, whereas $d(C_1-C_2) = 1.340$ Å in the isolated monomer. It is noteworthy that in the complex the three $C_\alpha-H$ distances are in the 1.100−1.101 Å range, while in the case of the CAM_{reac} reactant one of the hydrogen atoms displays a clear β-agostic interaction with the zirconium metal, having its $C_\alpha-H$ distance elongated to 1.133 Å, and a $Zr-H_\alpha$ distance of merely 2.394 Å, only 0.18 Å further from the metal than the α-carbon itself ($Zr-C_\alpha-H_\alpha$ angle of 84.6°).

The π-complex evolves to the insertion product through the TS labeled CAM_{TS}. In this TS a $Zr-C_\alpha$ bond breaks, a C_1-C_2 double bond turns into a single bond, and simultaneously two new bonds are formed: a $Zr-C_1$ one and a $C_\alpha-C_2$ one. The corresponding distances are $d(Zr-C_\alpha) = 2.315$ Å, $d(Zr-C_1) = 2.405$ Å, $d(C_1-C_2) = 1.417$ Å, and $d(C_\alpha-C_1) = 2.175$ Å. In this TS, one of the hydrogens on the α-carbon interacts again with the metallic center through an agostic effect, showing an elongation to 1.139 Å, and a Zr−H distance of only 2.167 Å.

The final product of this reaction features single $Zr-C_1$ (2.235 Å), C_1-C_2 (1.566 Å), and C_2-C_3 (1.561 Å) bonds, with a γ-H agostic interaction accounting for an

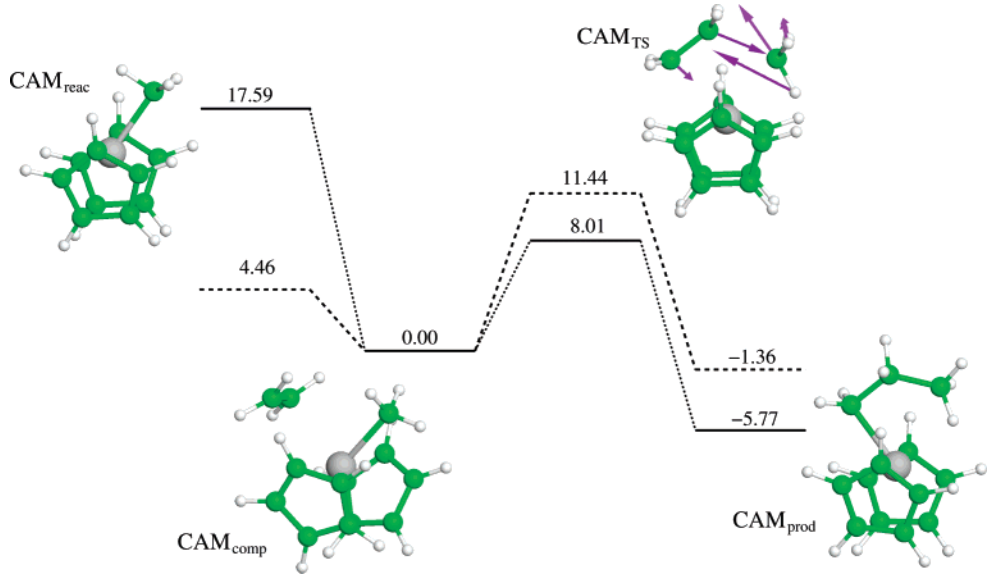

Figure 8. Stationary points along the Et + $[CH_3ZrCp_2]^+$ Cossée−Arlman reaction PES. Solid lines correspond to electronic energies, and dashed lines to Gibbs free energies, both values in kcal/mol at the B3LYP/TZ//B3LYP/LanL2DZdp level. The arrows in CAM_{TS} correspond to the motion of the atoms according to the normal mode with an imaginary frequency. The scale is arbitrary, but the relative moduli of the vectors match those of the Gaussian output.

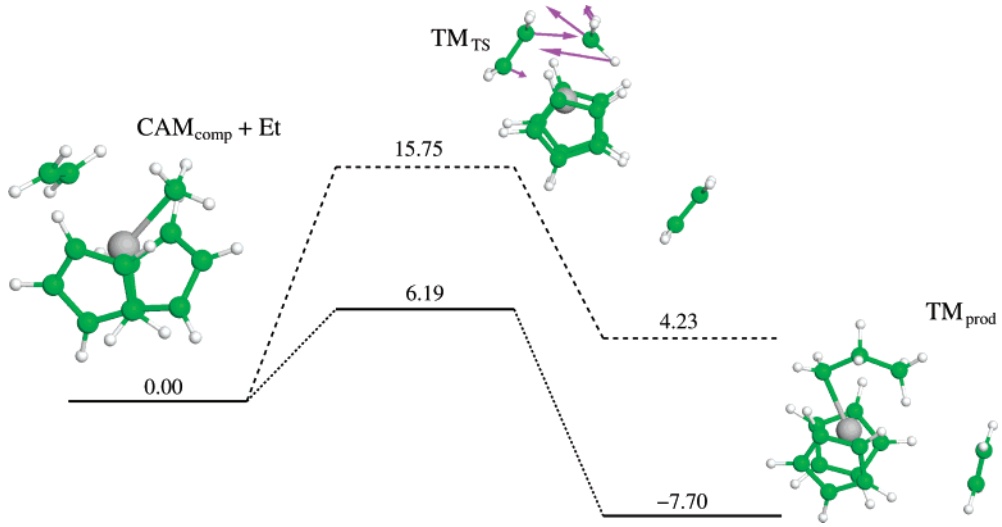

Figure 9. Stationary points along the Et + $[CH_3ZrCp_2]^+$ Trigger reaction PES. Solid lines correspond to electronic energies, and dashed lines to Gibbs free energies, both values in kcal/mol at the B3LYP/TZ//B3LYP/LanL2DZdp level. The arrows in TM_{TS} correspond to the motion of the atoms according to the normal mode with an imaginary frequency. The scale is arbitrary, but the relative moduli of the vectors match those of the Gaussian output.

elongation of the C_3-H_γ distance up to 1.127 Å, and a $Zr-H_\gamma$ distance of 2.262 Å.

For the TM, the reactants consist of an ethylene molecule plus the CAM_{comp} π-complex already calculated for the CAM reaction path and the corresponding TS (TM_{TS}) and product (TM_{prod}). These two species were also fully optimized at the B3LYP/LanL2DZdp theory level, and the corresponding geometries used for single-point calculations at the B3LYP/TZ level. These geometries and the Trigger mechanism energy profile are depicted in Figure 9. The energies are displayed in Table 2.

Table 2. Energy Differences and Gibbs Free Energy Differences (in kcal/mol) at Selected Stationary Points along the Trigger Reaction Path[a]

	LanL2DZdp		TZ	
species	ΔE	ΔG^{gas}	ΔE	ΔG^{gas}
CAM_{comp} + Et	0.00	0.00	0.00	0.00
TM_{TS}	4.97	14.52	6.19	15.75
TM_{prod}	−10.63	1.30	−7.70	4.23

[a] Values obtained by single-point calculations with the basis sets shown, on geometries optimized at the B3LYP/LanL2DZdp theory level.

A summary of the geometrical features of the TM reaction path follows. An ethylene monomer unit approaches the CAM_{comp} π-complex to form the insertion TS, without any intermediate complex to be found. In this TS, labeled TM_{TS}, the same bonds as in the CAM case are broken and formed. Here the corresponding distances are $d(Zr-C_\alpha) = 2.317$ Å, $d(Zr-C_1) = 2.405$ Å, $d(C_1-C_2) = 1.417$ Å, and $d(C_\alpha-C_1) = 2.174$ Å. In this TS, one of the hydrogens on the α-carbon interacts again with the metallic center through an agostic interaction,

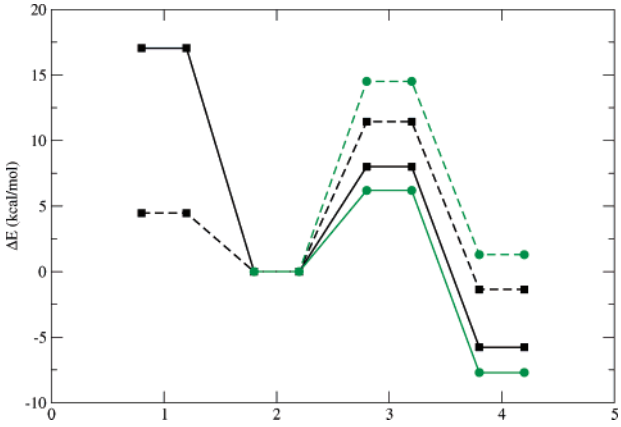

Figure 10. CAM (squares) and TM (circles) energy (continuous line) and Gibbs free energy (dashed lines) profiles.

showing an elongation to 1.139 Å, and a Zr−H distance of only 2.167 Å.

The final product of this reaction features single Zr−C_1 (2.239 Å), C_1−C_2 (1.564 Å), and C_2−C_3 (1.559 Å) bonds, with a γ-H agostic interaction accounting for an elongation of the C_3−H_γ distance up to 1.125 Å, and a Zr−H_γ distance of 2.272 Å.

The reaction energetics in Tables 1 and 2 are given with respect to the CAM_{comp} + Et reactants in the TM, but with respect to the CAM_{comp} complex in the CAM (and not the CAM_{reac} + Et reactants), as we want to compare barrier heights in both mechanisms. All energies are given in kcal/mol units.

The values for ΔE and ΔG are conveniently plotted in Figure 10.

Even if the TM is favored from an enthalpic point of view, the entropic effects of having a second monomer present in the transition state structure, instead of only one, make the system pay a high entropic toll. It is so high that the CAM turns out to be the mechanism with a lower Gibbs free energy barrier in the gas phase (4 kcal/mol lower).

Since the entropic contribution has been calculated via a harmonic approximation for the vibrational modes, doubt rises whether it has been overestimated, particularly due to many low-frequency normal modes present in the species of such a floppy system. These modes can hardly be well described under the harmonic approximation used in the present investigation. Regardless of this, the numbers are solid enough to make the point clear that there is some kind of trade off between the positive catalytic effect of the second monomer and the negative effect of the increased order of placing a second monomer molecule in the coordination sphere of the metal, or at least weakly bound to it.

4.2.3. Chain Flipping. This issue has been recently addressed from an experimental point of view,[52] as well as theoretically.[37,38] In our case, we have found a transition state, ind-Zc^{TS}, between two equivalent ind-Zc_1 minima, as depicted in Figure 11. This TS had a single imaginary frequency of 71i cm^{-1}. The low inversion barrier (vide infra) gives an idea of the flatness of the PES for the inversion. Visual inspection of the corresponding normal mode confirmed that it corresponds to the motion of the methyl group in the expected pseudoequatorial plane.

The calculated energetic barrier turns out to be 3.0 kcal/mol in electronic energy and 2.3 kcal/mol in Gibbs free energy, so with this model we would predict a very facile oscillation of the growing chain, if there is no other factor preventing it. The results in the paper by Goddard et al.[37] basically agree with ours: the geometrical minima are tetrahedral, not triangular planar (it would be a TS according to our calculations), but the energy difference is almost negligible.

Solvent effects are not expected to be important, since the charge arrangement is not significantly altered in the process, and the shape of the whole molecule is not drastically changed. Regarding this, one could think that for the long alkyl chain that is formed in the polymerization a huge volume of solvent is displaced by this flipping. But the important point is the movement of the chain "body" relative to the catalyst "head", so equivalently one could say that it is the zirconocene that is moving. The latter requires only minor solvent cavity distortion to occur; hence the relative energies within the solvent are expected to be similar to the vaccuum.

4.3. Inclusion of the Counterion. 4.3.1. Model Validation. Given the limited computational resources at hand, we have decided to mimic the $[CH_3B(C_6F_5)_3]^-$ species with a smaller moiety, namely, $[CH_3B(CF_2Cl)_3]^-$, guided by the following criteria.

First we took a CH_3B core that would bind through the CH_3 carbon to the zirconium atom in the metallocene, and then we chose three substituents Z (see Table 3) so that the properties of the resulting molecule $[CH_3BZ_3]^-$ would be as close as possible to the original $[CH_3B(C_6F_5)_3]^-$, both for the bare anion and for the complex formed with the $[CH_3ZrCp_2]^+$ fragment.

The substituents Z we have tested have been fluorine, chlorine, methyl, and the perfluoro/perchloro derivatives of the methyl and vinyl groups.

Table 3 summarizes the properties we have tested, at the B3LYP/LanL2DZdp level, for the bare anion and the complex.

It has to be noted that in the case of Z = $-CH_3$ the zirconocene cation would bind the methyl group more tightly than BZ_3, so that the resulting complex would not consist of an ion pair, but rather $Cp_2Zr(CH_3)_2$ + $B(CH_3)_3$.

To help choose the best-fitting model among the tested ones, we defined three errors ϵ as given in eqs 3, 4, and 5. In these equations, Δx refers to the difference, for property x, between the model and the original $[CH_3B(C_6F_5)_3]^-$ species.

$$5\epsilon_q^{\,2} = (\Delta q_B)^2 + (\Delta q_C)^2 + (\Delta q_C)^2 + (\Delta q_H)^2 + (\Delta q_{Zr})^2 \quad (3)$$

$$4\epsilon_d^{\,2} = (\Delta d_{B-C,anion})^2 + (\Delta\langle d_{C-H}\rangle)^2 + (\Delta d_{Zr-C})^2 + (\Delta d_{B-C,complex})^2 \quad (4)$$

$$\epsilon_{BE} = |\Delta BE| \quad (5)$$

The values for the errors according to definitions in eqs 3, 4, and 5 are tabulated in Table 4.

Inspection of Table 4 reveals that there is no single model that will beat all others, and our final choice will

(52) Busico, V.; Cipullo, R.; Cutillo, F.; Vacatello, M.; Castelli, V. V. A. *Macromolecules* (Communication) **2003**, *36* (12), 4258.

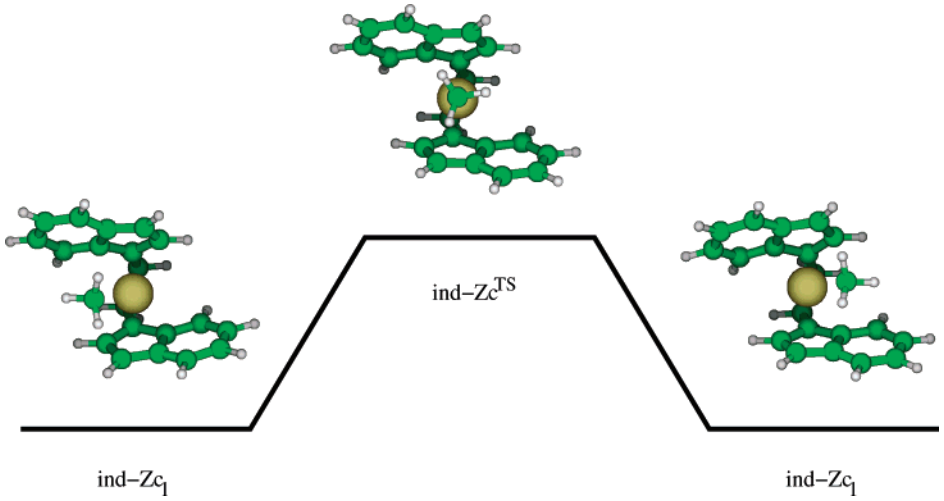

Figure 11. PES scheme for methyl flipping in *ansa*-ethylene-bis(indenil) methyl zirconium.

Table 3. Selected Properties of Some $[CH_3BZ_3]^-$ Models for the $[CH_3B(C_6F_5)_3]^-$ Counterion, at the B3LYP/LanL2DZdp Level[a]

	$[CH_3BZ_3]^-$					$[CH_3Cp_2Zr]^+/[CH_3BZ_3]^-$			
Z	q_B	q_C	$\langle q_H \rangle$	d_{B-C}	$\langle d_{C-H} \rangle$	q_{Zr}	d_{Zr-C}	d_{B-C}	BE
$-C_6F_5$	0.147	−0.434	0.109	1.647	1.099	0.590	2.528	1.689	−81.208
−Cl	0.172	−0.312	0.094	1.599	1.104	0.670	2.535	1.639	−86.824
−F	0.716	−0.482	0.069	1.615	1.103	0.751	2.519	1.675	−97.456
$-CH_3$	0.285	−0.446	0.041	1.661	1.108	1.273	2.292	4.451	−125.885
$-CCl_3$	0.816	−0.358	0.118	1.628	1.098	0.536	2.563	1.660	−81.020
$-CCl_2F$	0.587	−0.413	0.125	1.635	1.098	0.621	2.550	1.667	−81.487
$-CClF_2$	0.333	−0.440	0.121	1.644	1.100	0.602	2.533	1.650	−84.418
$-CF_3$	0.142	−0.469	0.111	1.632	1.100	0.615	2.532	1.657	−85.220
$-C_2Cl_3$	0.384	−0.473	0.128	1.656	1.098	0.541	2.530	1.702	−83.293
$-C_2Cl_2F$	0.360	−0.477	0.120	1.647	1.099	0.582	2.512	1.691	−85.319
$-C_2ClFCl$	0.319	−0.456	0.124	1.653	1.099	0.549	2.518	1.698	−85.489
$-C_2FCl_2$	0.057	−0.450	0.117	1.659	1.099	0.619	2.518	1.702	−84.639
$-C_2ClF_2$	0.340	−0.461	0.114	1.645	1.100	0.572	2.508	1.691	−87.630
$-C_2FClF$	0.042	−0.473	0.111	1.651	1.100	0.643	2.513	1.696	−86.058
$-C_2F_2Cl$	0.014	−0.446	0.112	1.657	1.100	0.623	2.511	1.702	−87.157
$-C_2F_3$	0.037	−0.468	0.104	1.651	1.101	0.639	2.509	1.698	−88.865

[a] Charges are given in electron units, distances in Å, and energies in kcal/mol. q_i stands for Mulliken atomic charge for atom i, for i = H, B, C, Zr. d_{i-j} stands for interatomic distance between atoms i and j, where i,j = H, C, B, Zr. BE stands for binding energy, as defined by $BE = E_{complex} - E_{cation} - E_{anion}$. $\langle q_H \rangle$ and $\langle d_{C-H} \rangle$ stand for the average values of both properties for the three quasi-equivalent hydrogen atoms in the methyl group of the CH_3B core.

Table 4. Relative Errors for the Different Models of the Counterion, According to Data from Table 3 and Formulas in Eqs 3, 4, and 5

Z	ϵ_q	ϵ_d	ϵ_{BE}
−Cl	0.067	0.035	5.615
−F	0.266	0.018	16.247
$-CH_3$	0.313	1.386	44.677
$-CCl_3$	0.302	0.025	0.188
$-CCl_2F$	0.197	0.017	0.279
$-CClF_2$	0.083	0.020	3.210
$-CF_3$	0.019	0.018	4.012
$-C_2Cl_3$	0.110	0.008	2.084
$-C_2Cl_2F$	0.097	0.008	4.110
$-C_2ClFCl$	0.080	0.007	4.281
$-C_2FCl_2$	0.043	0.010	3.431
$-C_2ClF_2$	0.087	0.010	6.422
$-C_2FClF$	0.056	0.008	4.849
$-C_2F_2Cl$	0.062	0.012	5.949
$-C_2F_3$	0.056	0.010	7.656

depend on the properties we regard most important, and how much so.

We started selecting the five models with smallest ϵ_{BE}, all of them below 3.5 kcal/mol. Although Z = $-CCl_3$ and Z = $-CCl_2F$ give binding energies very close to our reference molecule (ϵ_{BE} = 0.188 and 0.279, respectively), their errors in atomic charges (ϵ_q = 0.302 and 0.197, respectively) made us reject them.

We next decided to reject Z = $-C_2Cl_3$ and $-C_2FCl_2$, despite their good results (especially the latter), mainly because their slight increase in accuracy over the finally chosen one (Z = $-CClF_2$) would not justify their larger size and accordingly higher computational cost.

As a result, we chose Z = $-CClF_2$ as a good compromise between accuracy in both atomic charges, energetic and geometric parameters, and computational expense.

4.3.2. Et + $[CH_3ZrCp_2]^+/[CH_3B(CF_2Cl)_3]^-$ Scan Results. We have followed the same procedure as in Section 4.2.1, now including an explicit counterion, in the form of a $[CH_3B(CF_2Cl)_3]^-$ anion, as explained in Section 4.3.1. The resulting PES scan, at the B3LYP/SKBJ level, is displayed in Figure 12.

The first difference with respect to the bare cation case is that for $Zr-C_1C_2$ distances ranging from 6.0 to 3.55 Å the potential energy increases monotonically. Although there seems to be a π-complex formation at around $d(Zr-C_1C_2)$ = 2.9 Å (as in the bare cation case), the monomer has to overcome an energetic barrier in order to bind to the metal.

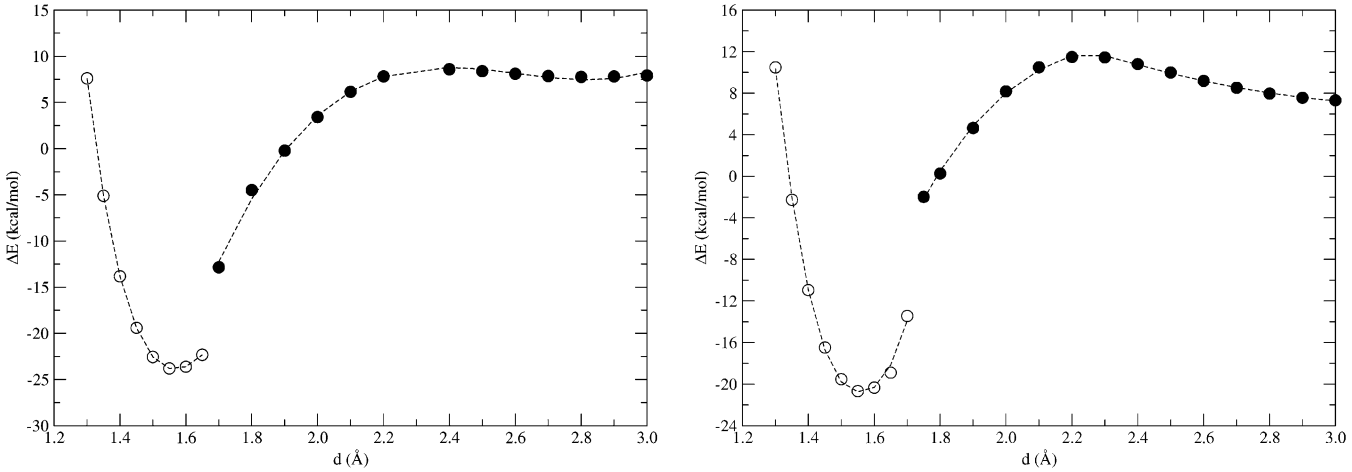

Figure 12. PES corresponding to varying the C_1-C_α (left) and $Zr-C_1C_2$ (right) distances for the ethylene + $[CH_3ZrCp_2]^+/[CH_3B(CF_2Cl)_3]^-$ system. In each plot open and solid black circles have been used to distinguish the two surfaces (see text), and the corresponding fitted functions are represented by dashed lines. Distances in Å and energies in kcal/mol.

Table 5. Fitted Constants for the Morse (first and third columns), Gaussian (second column), and Third-Order Polynomial (fourth column) Fits Corresponding, Respectively, to the π-Complex Basin, Monomer Approach to Zr, C_1-C_α Binding, and C_1-C_α Approach before Binding, for the Case of Et + $[CH_3ZrCp_2]^+/[CH_3B(CF_2Cl)_3]^-$[a]

ZrCC	basin	ZrCC	approach	CC	basin	CC	approach
A	7.2714	α	−1.66246	*A*	−21.0539	c_0	−532.441
B	16.4908	*β*	18.2988	*B*	375.221	c_1	644.126
C	1.30715	*γ*	0.944548	*C*	1.0006	c_2	−251.314
D	2.90584	*δ*	2.9915	*D*	1.55353	c_3	32.2016
R[a]	0.99968	*R*	0.99990	*R*	0.99883	*R*	0.99785

[a] The correlation coefficient between the fit and the calculated points.

This energy maximum seems to be the crossing point of two different energy surfaces, namely, the one corresponding to the π-complex basin from 2.50 to 3.50 Å, and the monomer approach basin, from 3.55 Å on. The different nature of the two surfaces is evident upon inspection of the $Zr-C_{CI}$ distance, where C_{CI} refers to the carbon atom in the methyl group of the counterion. In the complex basin $d(Zr-C_{CI})$ decreases from 4.57 Å at $d(Zr-C_1C_2) = 2.50$ Å, to 4.24 Å at $d(Zr-C_1C_2) = 3.50$ Å. On the other hand, at $d(Zr-C_1C_2) = 3.55$ Å, $d(Zr-C_{CI})$ jumps to a much shorter value of 3.22 Å, which evolves, as $d(Zr-C_1C_2)$ increases, to a constant $d(Zr-C_{CI}) = 2.58$ Å from $d(Zr-C_1C_2) = 4.80$ Å on.

In fact, these two PES fragments can be fitted with two relatively simple equations: a Morse-type potential for the π-complex basin and a Gaussian-type one for the approach channel, as displayed in eqs 6 and 7. The values of the constants for such equations are given in Table 5.

$$V_{\text{Morse}} = A + B(1 - e^{-C(x-D)})^2 \quad (6)$$

$$V_{\text{Gauss}} = \alpha + \beta e^{-\gamma(x-\delta)^2} \quad (7)$$

Some constants in the fitted functions bear a special meaning, which we will summarize next. In the case of the Morse fit to the complex basin, the parameter *D* stands for the distance where the minimum of the function is located, and thus corresponds to the $Zr-C_1C_2$ distance for the π-complex. Its energy is given by the value of parameter *A*.

In the case of the Gaussian fit to the monomer approach, the most remarkable parameter would be α, which gives us an idea of the basis set superposition error (BSSE), as this parameter should be exactly zero in its absence.

The electron deficiency that the zirconium atom had in the bare cationic species is now offset by the contribution of the counterion, so that the electron excess provided by the ethylene monomer, through its π-bond, is not required anymore. This fact generates a competition between nucleophiles (ethylene monomer vs $[CH_3B(CF_2Cl)_3]^-$ counterion), and thus the monomer has to overcome an effective "complexation barrier" before it can be inserted into the alkyl−metal bond.

The $d(C_1-C_\alpha)$ scan, on the other hand, suggests that once complexed, the insertion reaction crosses an energetic *plateau*, with a very low relative barrier for the cleavage of the methyl group and the formation of the new C−C and Zr−C bonds. Two PESs can also be distinguished in this plot: a binding zone at $d(C_1-C_\alpha) = 1.30-1.70$ Å and a C_1-C_α bond formation TS zone, from $d(C_1-C_\alpha) = 1.75$ Å on. The former has been fitted to a Morse-type function of the kind displayed in eq 6, and the latter to a third-degree polynomial, and the values of the parameters of such fits are also given in Table 5.

The key property here to tell one zone from the other is the $Zr-C_\alpha$ distance, which evolves from a constant value of 2.26 Å as the C_1 carbon approaches C_α up to around $d(C_1-C_\alpha) = 2.55$, where it starts to elongate to 2.72 Å at $d(C_1-C_\alpha) = 1.75$ Å. At $d(C_1-C_\alpha) = 1.70$ Å the α-carbon completely breaks its bond with the zirconium atom, jumping to a distance of 4.15 Å from it and staying always further than 4.5 Å at smaller C_1-C_α distances.

As in the case of the $d(Zr-C_1C_2)$ plot, some of the parameters have a special meaning. In the case of the binding basin, parameter D gives us the C_1-C_α equilibrium distance of the reaction product, and parameter A corresponds to its energy.

It is worth noting that, from the insertion TS on, the counterion takes its place back, provided that the coordination of the zirconium cation would otherwise drop formally to 3 again. While the $Zr-C_{CI}$ distance stays at around 4.5 Å for $d(C_1-C_\alpha)$ larger than 2.1 Å ,it drops to 2.58 Å for $d(C_1-C_\alpha)$ smaller than 1.70 Å with a rapid transition in between.

Stationary Points. As in the case of the bare cation, we have performed full geometry optimizations at the B3LYP/LanL2DZdp level at the relevant stationary points, namely, reactants, π-complex, complexation and insertion TSs, and product. Single-point energies have also been obtained, for the LanL2DZdp geometries, at the B3LYP/TZ level.

A summary of the geometrical features of these stationary points follows. In the MET_{reac} reactant only the α-carbon seems to be directly bound to the metal, with a $Zr-C_\alpha$ distance of 2.278 Å, although the carbon in the methyl group of the counterion is actually very close to the zirconium atom; that is, $d(Zr-C_{CI}) = 2.533$ Å. Unlike in the case of the counterionless CAM_{reac} reactant, here the longest $C_\alpha-H$ distance is only 1.101 Å, which points to an absence of agostic interaction with the metal center. Nevertheless the hydrogen atoms closest to the zirconium are those of the methyl group in the counterion. Two of them show a regular $d(C_{CI}-H) = 1.10$ Å distance and are 2.540 and 2.560 Å apart from the metal. The third hydrogen, however, is only 2.285 Å away from it and shows a noticeable $d(C_{CI}-H)$ elongation to 1.116 Å.

The monomer complexation occurs when an ethylene unit approaches the MET_{reac} catalyst ion pair, after crossing a complexation TS labeled MET_{TS1}. In this TS both carbons in the monomer and the one in the methyl group of the counterion are placed at similar distances from the Zr center, namely, $d(Zr-C_1) = 3.394$ Å, $d(Zr-C_2) = 3.344$ Å, and $d(Zr-C_{CI}) = 3.407$ Å. No α-agostic interaction is noticeable, with a longest $Zr-H_\alpha$ distance of 1.103 Å.

In the π-complex the Zr−C distances for the monomer carbons are 2.896 and 2.921 Å, and the $d(Zr-C\alpha)$ distance actually shortens from 2.278 Å in the reactant to 2.258 Å in the complex. At this stage the C_1-C_2 double bond is only slightly affected, with a C_1-C_2 distance of 1.350 Å, whereas $d(C_1-C_2) = 1.340$ Å in the isolated monomer. The counterion has left its place completely to the incoming monomer, with a $Zr-C_{CI}$ distance of 4.471 Å.

The π-complex evolves to the insertion product through the TS labeled MET_{TS2}. In this TS a $Zr-C_\alpha$ bond breaks, a C_1-C_2 double bond turns into a single bond, and simultaneously two new bonds are formed: a $Zr-C_2$ one and a $C_\alpha-C_1$ one. The corresponding distances are $d(Zr-C_\alpha) = 2.305$ Å, $d(Zr-C_2) = 2.442$ Å, $d(C_1-C_2) = 1.408$ Å, and $d(C_\alpha-C_1) = 2.229$ Å. In this TS, one of the hydrogens on the α-carbon interacts again with the metallic center through an agostic interaction, showing an elongation to 1.136 Å, and a H−Zr distance of only 2.189 Å. The counterion stays far from the metal, namely, $d(Zr-C_{CI}) = 5.316$ Å.

Table 6. Energy Differences (in kcal/mol) at Selected Stationary Points for the Insertion of Ethylene into $[CH_3ZrCp_2]^+/[CH_3B(CF_2Cl)_3]^-$ [a]

	LanL2DZdp		TZ	
species	ΔE	ΔG	ΔE	ΔG
$MET_{reac} + Et$	0.00	0.00	0.00	0.00
MET_{TS1}	16.45	27.07	18.06	28.68
MET_{comp}	13.52	22.80	15.04	24.32
MET_{TS2}	16.78	28.87	19.51	31.59
MET_{prod}	−20.38	−6.24	−16.40	−2.26

[a] Values obtained at the theory level shown, on B3LYP/LanL2DZdp geometries.

The final product of this reaction features single $Zr-C_2$ (2.299 Å), C_1-C_2 (1.542 Å), and C_2-C_3 (1.539 Å) bonds, with no γ-H agostic interaction in this case, because the propyl chain is oriented away from the metal.

The geometries, energy differences, and the potential energy profile so obtained are depicted in Figure 13, and the energies are given in Table 6.

4.3.3. Et + $[CH_3CH_2ZrCp_2]^+/[CH_3B(CF_2Cl)_3]^-$ Results. In this case we have followed the same procedure as in the case of the methylated catalyst. First a relaxed PES scan has been performed, and four regions have been differentiated, fitting them to four distinct functions. The results are depicted in Figure 14

It is evident from Figure 14 that the differences with the methylated case are quantitative, rather than qualitative. The four regions have been fitted to homologous functions, with the optimized parameters shown in Table 7.

Stationary Points. As in the case of the methylated zirconocene, the geometry optimizations have been performed at the B3LYP/LanL2DZdp level at the reactants, π-complex, complexation and insertion transition states, and product. Single-point energies have also been obtained, for the LanL2DZdp geometries, at the B3LYP/TZ level.

A summary of the geometrical features of these stationary points follows. In the ET_{reac} reactant only the α-carbon seems to be directly bound to the metal, with a $Zr-C_\alpha$ distance of 2.284 Å, although the carbon in the methyl group of the counterion is actually very close to the zirconium atom; that is, $d(Zr-C_{CI}) = 2.550$ Å. As in the case of the methylated MET_{reac} reactant, the hydrogen atoms closest to the zirconium are those of the methyl group in the counterion. One of them is only 2.275 Å away from it and shows a noticeable $d(C_{CI}-H)$ elongation to 1.116 Å.

The monomer complexation occurs when an ethylene unit approaches the ET_{reac} catalyst ion pair, after crossing a complexation TS labeled ET_{TS1}. In this TS both carbons in the monomer and the one in the methyl group of the counterion are placed at similar distances from the Zr center, namely, $d(Zr-C_1) = 3.347$ Å, $d(Zr-C_2) = 3.320$ Å, and $d(Zr-C_{CI}) = 3.433$ Å. No α-agostic interaction is noticeable, with both α-hydrogens at a Zr−H distance of 1.104 and 1.106 Å.

In the π-complex the Zr−C distances for the monomer carbons are 2.766 and 2.827 Å, and the $d(Zr-C_\alpha)$ distance actually shortens from 2.284 Å in the reactant

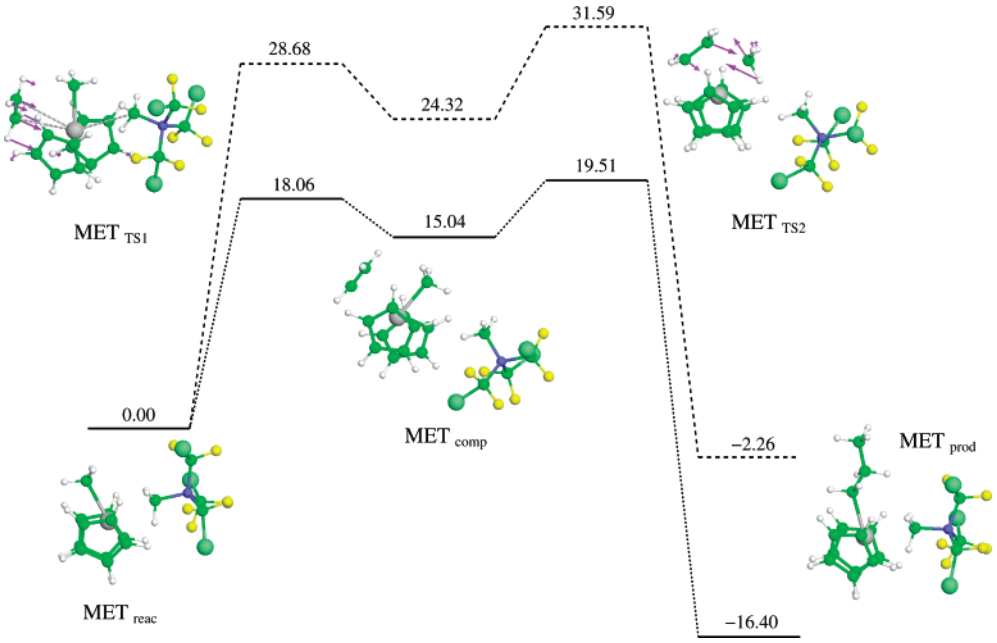

Figure 13. Stationary points along the Et + $[CH_3ZrCp_2]^+/[CH_3B(CF_2Cl)_3]^-$ reaction PES. Solid lines correspond to electronic energies, and dashed lines to Gibbs free energies, both values in kcal/mol at the B3LYP/TZ//B3LYP/LanL2DZdp level. The arrows in MET_{TS1} and MET_{TS2} correspond to the motion of the atoms according to the normal mode with an imaginary frequency. The scale is arbitrary, but the relative moduli of the vectors match those of the Gaussian output.

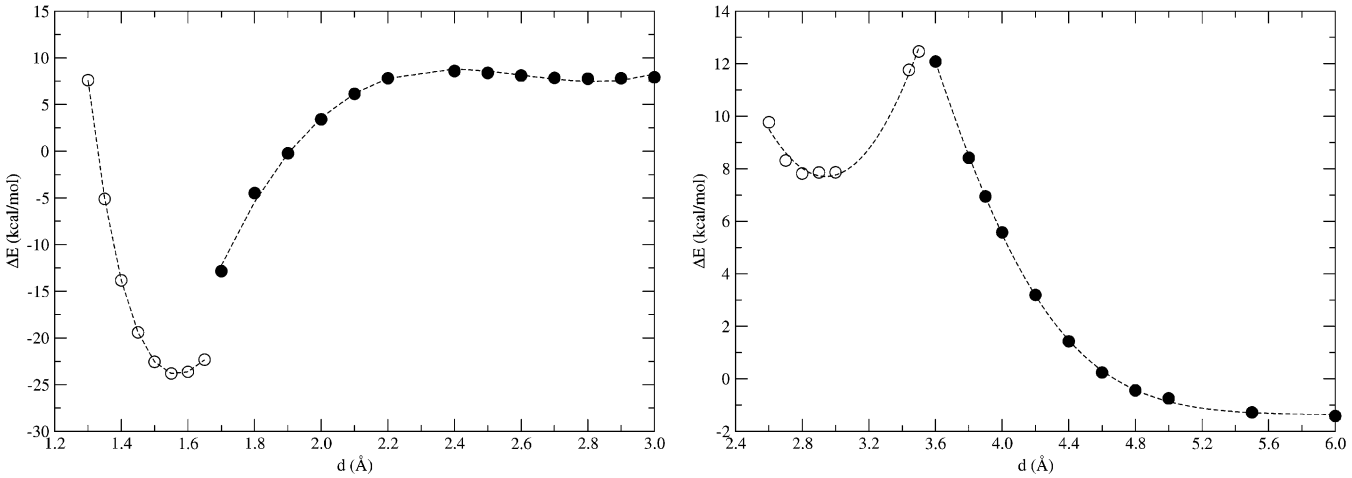

Figure 14. PES corresponding to varying the C_1-C_α (left) and $Zr-C_1C_2$ (right) distances for the ethylene + $[CH_3CH_2ZrCp_2]^+/[CH_3B(CF_2Cl)_3]^-$ system. In each plot open and solid black circles have been used to distinguish the two surfaces (see text), and the corresponding fitted functions are represented by dashed lines. Distances in Å and energies in kcal/mol.

Table 7. Fitted Constants for the Morse (first and third columns), Gaussian (second column), and Third-Order Polynomial (fourth column) Fits Corresponding, Respectively, to the π-Complex Basin, Monomer Approach to Zr, C_1-C_α Binding, and C_1-C_α Approach before Binding, for the Case of Et + $[CH_3CH_2ZrCp_2]^+/[CH_3B(CF_2Cl)_3]^-$

ZrCC	basin	ZrCC	approach	CC	basin	CC	approach
A	7.68114	α	−1.37113	*A*	−23.8808	c_0	−563.395
B	25.4299	*β*	28.14398	*B*	72.7367	c_1	666.88
C	0.90796	*γ*	0.669329	*C*	1.89426	c_2	−257.534
D	2.87488	*δ*	2.54886	*D*	1.56691	c_3	32.9195
R^a	0.99879	*R*	0.99991	*R*	1.00000	*R*	0.99834

[a] Correlation coefficient between the fit and the calculated points.

to 2.243 Å in the complex. At this stage the C_1-C_2 double bond is slightly elongated, with a C_1-C_2 distance of 1.359 Å, whereas $d(C_1-C_2) = 1.340$ Å in the isolated monomer. The counterion has left its place completely to the incoming monomer, with a $Zr-C_{Cl}$ distance of 4.368 Å.

The *π*-complex evolves to the insertion product through the TS labeled ET_{TS2}. In this TS a $Zr-C_\alpha$ bond breaks, a C_1-C_2 double bond turns into a single bond, and simultaneously two new bonds are formed: a $Zr-C_2$ one and a $C_\alpha-C_1$ one. The corresponding distances are $d(Zr-C_\alpha) = 2.310$ Å, $d(Zr-C_2) = 2.475$ Å, $d(C_1-C_2) =$

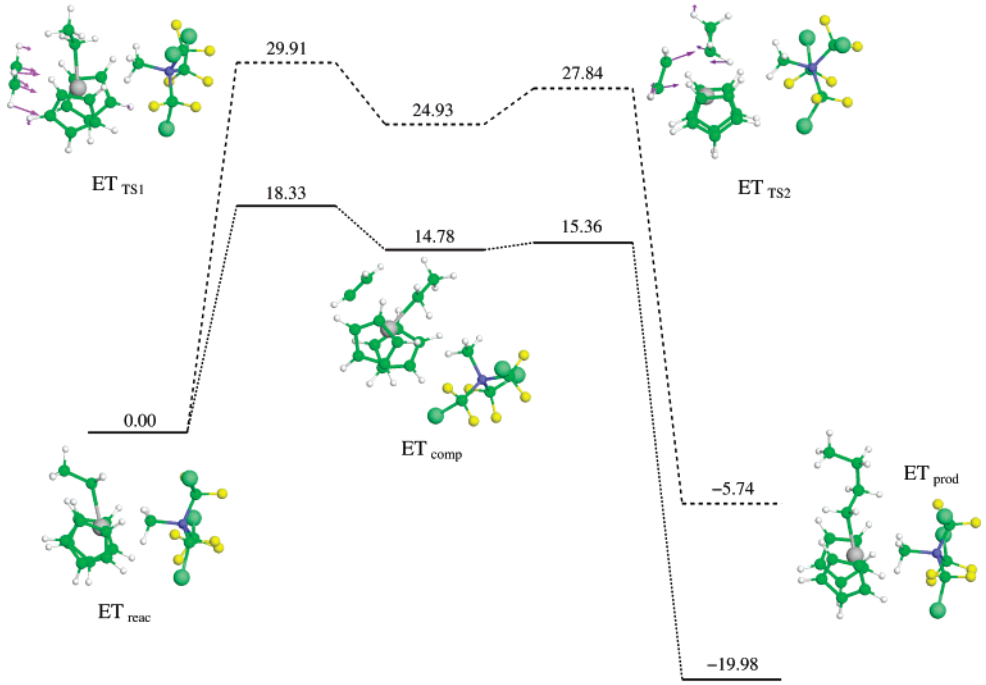

Figure 15. Stationary points along the Et + $[CH_3ZrCp_2]^+/[CH_3B(CF_2Cl)_3]^-$ reaction PES. Solid lines correspond to electronic energies, and dashed lines to Gibbs free energies, both values in kcal/mol at the B3LYP/TZ//B3LYP/LanL2DZdp level. The arrows in ET_{TS1} and ET_{TS2} correspond to the motion of the atoms according to the normal mode with an imaginary frequency. The scale is arbitrary, but the relative moduli of the vectors match those of the Gaussian output.

Table 8. Energy Differences (in kcal/mol) at Selected Stationary Points for the Insertion of Ethylene into $[CH_3CH_2ZrCp_2]^+/[CH_3B(CF_2Cl)_3]^-$ [a]

	LanL2DZdp		TZ	
species	ΔE	ΔG	ΔE	ΔG
ET_{reac} + Et	0.00	0.00	0.00	0.00
ET_{TS1}	16.72	28.30	18.33	29.91
ET_{comp}	12.93	23.08	14.78	24.93
ET_{TS2}	−12.98	25.46	15.36	27.84
ET_{prod}	−23.30	−9.06	−19.98	−5.74

[a] Values obtained at the theory level shown, on B3LYP/LanL2DZdp geometries.

1.400 Å, and $d(C_\alpha-C_1) = 2.319$ Å. In this TS, one of the hydrogens on the α-carbon interacts again with the metallic center through an agostic interaction, showing an elongation to 1.144 Å, and a Zr−H distance of only 2.127 Å. The counterion stays far from the metal, namely, $d(Zr-C_{Cl}) = 4.380$ Å.

The final product of this reaction features single $Zr-C_2$ (2.297 Å), C_1-C_2 (1.542 Å), C_1-C_3 (1.546 Å), and C_3-C_4 (1.534 Å) bonds, with no γ-H agostic interaction in this case, because the butyl chain is oriented away from the metal.

The geometries, energy differences, and potential energy profile so obtained are depicted in Figure 15, and the energy differences are summarized in Table 8.

5. Conclusions

5.1. Bare Cation. Our quantum chemical results entitle us to shed some light on the questions posed previously. As we will see, the TM gives straightforward and simple answers to the three of them, but with the CAM, they are not so obvious.

The first question deals with the reaction rate order with respect to the monomer. Of course, all the considerations have to be made taking into account the free energy surface, as that is the surface traveled in any chemical reaction, as mentioned above.

Inspection of the mechanism proposed by Ystenes (see Figure 9) leads directly to a kinetic equation in close agreement with what is experimentally known. The reaction has only one step, and it is bimolecular.

In the case of the CAM, the closeness in free energy of the reactants and the complex (species CAM_1 + Et and CAM_2) and the absence of a classic transition state between them suggest that a very fast preequilibrium exists. In that case, bimolecularity of the whole reaction (i.e., first order of reaction rate with respect to both catalyst and monomer) could be derived. Recall that our electronic energy barrier for ethylene insertion (7.7 kcal/mol) and reaction exothermicity (22 kcal/mol) are in good agreement with the values by Morokuma et al.[10] for a silylene-bridged zirconocene (less than 10 kcal/mol barrier, and around 30 kcal/mol exothermicity), but we go one step further, calculating ΔG, which gives us a different picture of the reaction. First, the free energy barrier is different (higher), and second the π-complex results at almost the same free energy as the reactants.

In the case of the chain flipping, the energy barrier we get for the system considered is so low that the position of the growing chain should be expected to be random, equally distributed between both coordination sites. If experimental results make it unacceptable, then either any model that leaves a coordination site empty in some reaction step (e.g., CAM) must be discarded or our model is too simple to account for some important subtleties that fix the growing chain in place (even when the other coordination site is empty). It is important to note, though, that, as mentioned in Section 2, there are some known metallocenic catalytic systems for which a facile chain inversion is indeed deduced from experi-

ment.[38] Thus, Mohammed et al. mention two limit cases. When the chain inversion (flipping) rate is much higher than the monomer insertion one, Curtin−Hammet (CH) conditions are invoked. In this case, both states are fully equilibrated. When the opposite is true (insertion much faster than inversion), they use the term kinetic quenching (KQ). Our calculations predict CH conditions for the case under study, but KQ catalytic systems must exist in order to obtain syndiotactic polymers. In the latter case, the mechanistical explanation Mohammed et al. give is that the effect of the counterion is to bind more or less strongly to the metallocene cation and consequently to obstruct such inversion. In the case where the binding is stronger, the tacticity will increase (KQ conditions), but the polymerization rate will decrease (it will be harder for the incoming monomer to take the counterion's place).

Regarding the effect of other Lewis bases, we can conclude that their effect must be similar to that of the counterion we mention above. Small amounts of Lewis bases present will increase tacticity and decrease propagation rate, although their effect will be significant only when the counterion is loosely bound to the metallocene cation (CH conditions) and will be masked by the counterion itself when it binds more strongly (closer to KQ conditions). These ideas do not collide with those by Vanka and Ziegler.[34]

5.2. Inclusion of Counterion. As mentioned in Section 4.3.1, the binding energy of the counterion is around 81 kcal/mol (in the gas phase), which makes it rather unlikely that immersed in such an apolar solvent as *n*-heptane or other typical olefin polymerization media the bare cation could be regarded as the active species. The results presented in the second part of the paper are thus more representative of the reaction medium.

Having found two TSs in either PES is quite revealing, and further clarification is obtained by the fact that both TSs are really close in energy. In fact, in the ethylated case the insertion barrier has an absolute height 3 kcal/mol *lower* than the complexation one. These data can help us understand why the reaction kinetics obey a first-order law with respect to both catalyst and monomer (overall second-order kinetics). It is so because the complexation step has a barrier much higher than that from the complex to the products, or, in other words, the complexation is the limiting step, not the insertion. Our results concur with similar propositions by other authors.[53]

The picture we get when including the counterion is thus a hybrid of both CAM and TM. On one hand, the reaction proceeds in a two-step fashion, through a complexation and subsequent insertion, as hypothesized by Cossée and Arlman. On the other hand, the insertion TS is affected by the presence of a second electron donor, as Ystenes proposed in his Trigger mechanism, although this electron donor would be the counterion itself, and not a second monomeric unit.

The effect of the Lewis bases is also evident within this framework: the complexation step can and will be traversed by other (not the monomer) Lewis bases, but it will be reversible, since only the monomer will proceed to insertion. That is why Lewis bases can reduce slightly the polymerization rate (they "occupy" a fraction of the catalyst), but do not inhibit the catalyst action.

With regard to the side-chain flipping, we have to admit that the reaction path presented here would lead, apparently, to a polymer growth where the chain would always remain in the same coordination site of the metal. This would fit into a "chain stationary" insertion type described by some authors.[25] However further study needs to be done on chain inversion mechanisms and barriers.

In summary, we have pointed out the importance of calculating Gibbs free energy profiles, in adition to the usual electronic energy ones, to give insight into the reaction path followed by the system under study, as well as including the counterion into the calculations.

We conclude that detailed energetic calculations are imperative in such systems, provided that there are two TSs apparently very close in energy.

Acknowledgment. This research was funded by Euskal Herriko Unibertsitatea (the University of the Basque Country), Gipuzkoako Foru Aldundia (the Provincial Government of Gipuzkoa), and Eusko Jaurlaritza (the Basque Government). I.S. thanks Eusko Jaurlaritza for a grant. I.S. also thanks Prof. Rafael R. Pappalardo for fruitful help with computational details. The SGI/IZO-SGIker UPV/EHU (supported by Fondo Social Europeo and MCyT) is gratefully acknowledged for generous allocation of computational resources.

Supporting Information Available: Complete refs 13 and 39 (PDF). This material is available free of charge via the Internet at http://pubs.acs.org.

OM0503139

(53) Vanka, K.; Xu, Z.; Ziegler, T. *Organometallics* **2004**, *23* (12), 2900.